

# A shift in the Sr isotopic composition of the magmatic source triggering 2019 paroxysmal eruptions at Stromboli Volcano

Renggli C.J., Krause J., Genske F., Gilbricht S., Gattuso A., Böhnke M., Berndt J., Giuffrida G.B.

5

This manuscript is a non-peer reviewed preprint submitted to EarthArXiv  
The manuscript is under review in the Journal Volcanica

10

Renggli: <https://orcid.org/0000-0001-8913-4176> [renggli@mps.mpg.de](mailto:renggli@mps.mpg.de) Twitter: @crenggli

Krause: [joachim.krause@hzdr.de](mailto:joachim.krause@hzdr.de)

Genske: <https://orcid.org/0000-0002-7520-0184> [felix.genske@uni-muenster.de](mailto:felix.genske@uni-muenster.de) Twitter: @FelixGenske

Gilbricht: <https://orcid.org/0000-0003-1113-2415> [sabine.gilbricht@mineral.tu-freiberg.de](mailto:sabine.gilbricht@mineral.tu-freiberg.de)

15 Gattuso: <https://orcid.org/0000-0003-1815-0421> [alessandro.gattuso@ingv.it](mailto:alessandro.gattuso@ingv.it)

Böhnke: <https://orcid.org/0000-0002-3875-2086> [mischa.boehnke@uni-muenster.de](mailto:mischa.boehnke@uni-muenster.de)

Berndt: <https://orcid.org/0000-0002-6766-3066> [jberndt@uni-muenster.de](mailto:jberndt@uni-muenster.de)

Giuffrida: <https://orcid.org/0000-0003-3497-2759> [giovanni.giuffrida@ingv.it](mailto:giovanni.giuffrida@ingv.it)

## ABSTRACT

The persistent volcanic activity of Stromboli Volcano, Aeolian Islands, Italy, is interrupted by paroxysmal eruptions on a decadal interval. In 2019, two strong paroxysms on July 3<sup>rd</sup> and August 28<sup>th</sup>, ended a more than a decade long period of regular strombolian activity. During normal strombolian activity the volcano erupts highly porphyritic scoria and lava (HP) with a shoshonitic basalt composition. In paroxysmal eruptions the HP material is mingled with low porphyritic (LP) pumices. Here, we provide new in-situ chemical measurements of the glass phases of LP and HP materials. We also provide the first radiogenic isotope data on the bulk compositions of the LP and HP components erupted on July 3<sup>rd</sup>, 2019. These data show a remarkable shift in the Sr isotope ratio of the LP reservoir to more radiogenic compositions, not observed since the paroxysm in 1930.

## 10 SECOND-LANGUAGE ABSTRACT

L'attività vulcanica persistente che caratterizza il vulcano Stromboli, Isole Eolie, Italia, viene interrotta, con cadenza decennale, da eruzioni di tipo parossistico. Nel 2019 due forti parossismi avvenuti rispettivamente il 3 luglio e il 28 agosto hanno interrotto un periodo di attività stromboliana che durava da oltre dieci anni. Durante l'ordinaria attività stromboliana il vulcano erutta scoria e lava altamente porfirica (HP) con composizione basaltica shoshonitica. Nelle eruzioni parossistiche il materiale HP si mescola con pomici a bassa porfiricità (LP). In questo lavoro proponiamo nuove misure chimiche in situ delle fasi vetrose dei materiali LP e HP. Inoltre, forniamo i primi dati isotopici radiogenici sulle composizioni di massa dei componenti LP e HP eruttati il 3 luglio 2019. Questi dati mostrano un notevole spostamento del rapporto isotopico dello Sr del serbatoio LP verso composizioni più radiogeniche, che non si osservava dai tempi del parossismo del 1930.

## 20 1 INTRODUCTION

Stromboli volcano (Aeolian Islands, Italy) is a textbook example of an active steady-state stratovolcano. Strombolian eruptions occur at intervals, as short as 5 minutes during phases of high activity (Rosi et al. 2013). However, the eruptive history of the last century shows that the steady-state eruptive behavior is occasionally interrupted by explosive paroxysms. Since the beginning of the 21<sup>st</sup> century major paroxysms occurred on the 5<sup>th</sup> of April 2003, 15<sup>th</sup> of March 2007, and on the 3<sup>rd</sup> of July and 28<sup>th</sup> of August 2019. The paroxysmal eruption in 2003 followed a relatively quiescent period, as no large-scale paroxysms occurred since 1959. From 1906-1959 a total of 16 paroxysms were recorded, triggering 5 tsunami events (Bevilacqua et al. 2020; Rosi et al. 2013). These irregular explosive eruptions highlight the hazardous potential of normally steady-state eruptions, which are an important touristic attraction. It is therefore imperative to constrain the mechanisms of paroxysmal eruptions. Here, we present major and trace element data on mineral and glass compositions of the erupted materials, and radiogenic isotope compositions of the mingled magma components.

The strombolian activity is characterized by the eruption of crystal-rich, black scoria, commonly referred to as highly porphyritic (HP) magma. In paroxysmal eruptions the HP magma is mingled with crystal poor, light-brown pumice,

labelled low porphyritic (LP) magma and also referred to as golden pumice (Bertagnini et al. 1999, 2003; D’Oriano, Bertagnini, and Pompilio 2011; Francalanci, Tommasini, and Conticelli 2004; Lautze and Houghton 2005; Métrich et al. 2005; Viccaro et al. 2021). The whole-rock compositions of the HP and LP magmas fall on the border between high-K basalts and shoshonitic basalts, with SiO<sub>2</sub> concentrations of 48.5-51.5 wt.% in the HP magma, and 48-50 wt.% in the LP magma (Bertagnini et al. 2008; Francalanci et al. 2008; Landi et al. 2004, 2006, 2008; Métrich et al. 2001). The glassy matrix of the more extensively crystallized HP scoria has SiO<sub>2</sub> concentrations of 51-53 wt.% and is shoshonitic in composition, whereas the LP glass overlaps in composition with the HP whole rock (Bertagnini et al. 2008; Landi et al. 2006, 2008). Crystal contents in the HP magma range from 38-55 vol.%, with 22-35 vol.% plagioclase, 5-20 vol.% clinopyroxene and 2-9 vol.% olivine (Allard 2010; Landi et al. 2006; Métrich, Bertagnini, and Muro 2010), whereas the LP magma has a crystal content of less than 5 vol.% of clinopyroxene and olivine (Bertagnini et al. 2003; Métrich et al. 2010).

The Stromboli plumbing system is described as a vertically overlying sequence of magma ponding reservoirs that are connected by dikes. A lower magmatic ponding chamber at a depth of 7-10 km below the summit is proposed to host the LP magma, and the more evolved HP magma resides in a shallow plumbing system at 2-4 km below the summit (Métrich et al. 2010). The general eruption trigger is explained by the slow accumulation of a CO<sub>2</sub> rich gas-phase that propels LP magma into the shallow HP reservoir, where the two magmas mingle and drive large paroxysmal eruptions. In between paroxysmal eruptions small quantities of LP magma move into the shallow reservoir, without triggering explosions, where the magma loses H<sub>2</sub>O, promoting plagioclase crystallization and the formation of the crystal-rich HP magma. This HP magma continuously erupts in steady state strombolian activity. The homogeneous nature of the HP lavas over time suggests efficient mixing, where the timescales of homogenization are shorter than the residence time in the HP reservoir (Di Stefano et al. 2020; Francalanci et al. 1999).

The major and trace element compositions, including Sr concentrations, of the LP and HP magmas have remained constant over the past century. However, the Sr isotopic ratio (<sup>87</sup>Sr/<sup>86</sup>Sr) has decreased starting in the early 1980s (Bertagnini et al. 2008; Francalanci et al. 1999, 2005, 2004). The decrease in <sup>87</sup>Sr/<sup>86</sup>Sr of the HP lavas predates a large lava flow eruption in December 1985 (Francalanci et al. 1999). In this study, Francalanci et al. (1999) discussed possible reasons for the change in the Sr-isotopic composition, discarding assimilation of unradiogenic country rock or gradual changes in the source magma. Instead, they suggest a distinct change in the isotopic composition of the LP input magma feeding the HP reservoir, prior to the 1985 lava flow eruption (Francalanci et al. 1999). Here, we extend the record of time dependent <sup>87</sup>Sr/<sup>86</sup>Sr variation for both LP and HP materials to the paroxysmal eruptions in July and August 2019.

30

## 2 METHODS

### 2.1 Electron Probe Microanalysis (EPMA)

Quantitative analyzes of olivine, clinopyroxene, plagioclase and glass were performed along transects and on single spots with a JEOL JXA 8530 F Hyperprobe at the Helmholtz Institute Freiberg for Resource Technology, Germany using all five wavelength dispersive spectrometers (WDS). An acceleration voltage of 20 kV, a probe current of 20 nA and spot sizes between 1 and 5  $\mu\text{m}$  were chosen for the minerals. Glasses were measured with an acceleration voltage of 15 kV a probe current of 12 nA and beam diameters between 5 and 10  $\mu\text{m}$ . Measured concentrations were corrected offline for instrument drift, measuring natural mineral reference materials (ASTIMEX MIN25), and mutual interferences were corrected ( $V_{\text{K}\beta}$  on  $\text{Cr}_{\text{K}\alpha}$ ,  $\text{Ti}_{\text{K}\beta 1,3}$  on  $\text{Ba}_{\text{L}\beta}$ ,  $\text{Cr}_{\text{K}\beta}$  on  $\text{Mn}_{\text{K}\alpha}$  and  $\text{Cr}_{\text{K}\alpha 3\text{rd order}}$  on  $\text{Sr}_{\text{L}\alpha}$ ) (Osbahr et al. 2015). Values below the lower limit of quantification as well as with relative 2SD above 40% have been omitted from the dataset.

## 2.2 SEM-Based automated Mineralogy

The phase distribution in polished thin sections was measured with a SEM Quanta 600F from FEI at the Technical University Freiberg. The SEM is equipped with the MLA (Mineral liberation analyser) software package for automated SEM-based mineral identification of ThermoFisher SCIENTIFIC former FEI (Schulz et al. 2020, Fandrich et al. 1997). To account for the fine-grained texture of the samples we measured the sections with a high resolution of 1000x1000 pixel and a pixel size of  $1\mu\text{m}^2$  in the GXMAP mode.

## 2.3 Laser Ablation Inductively Coupled Plasma Mass Spectrometry (LA-ICP-MS)

Trace element concentrations glasses were determined with LA-ICP-MS. The measurements were performed in the LA-ICP-MS laboratory at the Institute at for Mineralogy, Universität Münster, Germany. A Teledyne Photon Machines Analyte G2 193 nm Excimer LASER ablation system is coupled to a Thermo Scientific Element XR double focusing sector field mass spectrometer.  $^{43}\text{Ca}$  was used as internal standard. The relative sensitivity factors for all other masses were determined with NIST612, which was also used to tune the instrument for high intensities on La and Th and low oxide rates ( $\text{ThO}/\text{Th} < 0.002$ ). Concentrations were calculated using a 2-stage Excel-based spreadsheet. Values below the lower limit of quantification were excluded. The accuracy has additionally been monitored by the repeated analysis of the GSD-1G and GSE-1G reference materials.

## 2.4 Isotopic analysis

The radiogenic isotope ratios (Sr-Nd-Hf-Pb) of the LP and HP samples were analyzed at the Institut für Mineralogie at the University of Münster on a Thermo Scientific Neptune *Plus* MC-ICP-MS. LP and HP materials were carefully picked to preclude cross-contamination between the end-member components. The rock powders were leached in cold 6 N HCl in an ultrasonic bath for 2h and rinsed three times with Milli-Q  $\text{H}_2\text{O}$ . The dried samples were digested in Savillex® Teflon vials at  $120^\circ\text{C}$  for 2 days using mixtures of concentrated, double-distilled HF and  $\text{HNO}_3$ . Boric acid and 6 N HCl were added throughout the digestion procedure to aid the removal of fluorides.

After full dissolution, clear sample solutions were separated on standard cation (Biorad® AG50W X-8) columns to separate HFSE, Sr and the REE fractions (Genske et al. 2012). The HFSE fraction was then loaded onto Eichrom Ln

Spec columns to separate Hf (Münker et al. 2001). The REE cut from the cation column was further purified for Nd using standard (Eichrom®, 50-100 µm) Ln Spec chromatography protocols (Pin and Zalduegui 1997). We further applied protocols for Tl-doped Pb isotope analyses via MC-ICP-MS (Lugmair and Galer 1992; Todd, Stracke, and Scherer 2015). For the Sr isotope measurements, a purification column using Sr spec resin was applied to remove residual, fractionated Rb from the sample solution, to measure sample loads of pure Sr (about 10 ng) by MC-ICP-MS. To verify accuracy and precision of the Sr MC-ICP-MS analytics, aliquots of BCR-2 and BHVO-2 were measured (dataset, Renggli et al. 2023) along with the samples, and Sr isotope measurements were normalized to NBS 987 with  $^{87}\text{Sr}/^{86}\text{Sr} = 0.710248$ , which was run as a bracketing standard after 3-4 sample measurements.

For the Hf isotope measurements, Lu and Yb contributions onto corresponding Hf masses were generally below 0.5 and 5 µg/g. However, performing a clean-up separation scheme using the same columns yields Hf cuts with less than 1 µg/g Yb contributions. All measured Hf isotope ratios were normalized to Ames  $^{176}\text{Hf}/^{177}\text{Hf} = 0.282160$ , which is isotopically indistinguishable from JMC-475 (Blichert-Toft, Chauvel, and Albarède 1997). For Nd the reference material BCR-2 was measured at 5 ppb and 20 ppb Nd dilutions.

All isotope data determined for USGS reference materials are in excellent agreement with reported literature values (Weis et al. 2006) and the recommended GeoReM values (Jochum et al. 2005). The measurement results of BCR-2, BHVO-2, and NBS 987 are reported in the dataset (Renggli et al. 2023). The reference materials were prepared by the same chemical separation procedures as the whole rock samples. Isotope data of the samples are summarized in Table 2 and given in detail in the dataset on the DIGIS Geochemical Data Repository (Renggli et al., 2023).

### 20 3 RESULTS

We collected hand-sized scoria samples near the summit Pizzo Sopra la Fossa, from which we prepared thin sections (S1, S3 and S4 presented in this manuscript). The samples prepared as thin sections were selected to represent the different degrees of mingling of the LP and HP magmas observed in the hand samples. The HP magma is distinguished by the dark, black color, and the high abundance of crystals, with sizes ranging up to 5 mm. The LP magma has a light beige-brown color and is crystal poor. Thin section S1 represents the LP endmember (Figure 1), and thin section S4 represents the HP endmember (Figure 2). S3 shows mingled textures with near-equal amounts of HP and LP magma, shown in Figure 3. Table 1 shows the major and trace element composition of the glass phases in the HP and LP magmas. These compositions are not distinguishable from those measured in the eruption products of the paroxysms in 2003 and 2007 (Métrich et al. 2010). The chemical similarity of the pumices and scoria erupted in 2019 can be exemplified by a comparison of the Sc and Rb concentrations in the matrix glasses with previously reported data. The LP pumices erupted in 2019 have a Sc concentration of  $27.8 \pm 0.7$  µg/g and a Rb concentration of  $54.8 \pm 1.5$  µg/g. The Sc concentration falls in the field of 1996-2000 pumices (24-32 µg/g) and is moderately higher than that of the pumices erupted on April 5<sup>th</sup>,

2003 (Francalanci et al. 2008). Whereas the Rb concentration of the pumices falls in the same range as the 1996-2000 and the 2003 pumices (40-100  $\mu\text{g/g}$ ). The HP glass erupted in 2019 has a Sc concentration of  $23.7\pm 0.8$   $\mu\text{g/g}$  and a Rb concentration of  $136.5\pm 6.6$   $\mu\text{g/g}$ , which falls in the range of concentrations reported for 1996-2000 and 2003 paroxysmal scoria, at 20-30  $\mu\text{g/g}$  Sc and 110-150  $\mu\text{g/g}$  Rb (Francalanci et al. 2008).

5 The low porphyritic pumice is very crystal-poor and bubble-rich. A quantitative analysis of the phase distribution observed by MLA (Figure 1) gives a LP glass content of  $\sim 30$  area% and 65% bubbles. The thin section S1 contains less than 1% HP glass, and approximately 1% each of plagioclase, olivine, and clinopyroxene. The plagioclase crystals hosted in the LP melt are anorthite-rich ( $\text{An}_{91}$ ) and heavily resorbed with sieve textures (Armienti, Francalanci, and Landi 2007). Olivines hosted in the LP magma include two groups, with the first characterized by zonations, abundant melt inclusions,  
10 and a  $\text{Mg\#} \sim 77$  in the core, and the second group of olivines are homogeneous and have a  $\text{Mg\#} = 85$ . The clinopyroxenes are commonly sector-zoned, with  $\text{Mg\#}$  in the sectors of 82 and 85. Additionally, some clinopyroxenes have resorbed cores with lower  $\text{Mg\#} \sim 68$ .

The high porphyritic scoria (S4) and lava flow samples consist of 28-35% glass (Figure 2). The bubble content ranges from 30-40%, with the scoria at the higher end of the range at 40%. Plagioclase is the most abundant mineral phase with  
15 18-25%, followed by clinopyroxene at 6-10%, and 3% olivine. The plagioclase crystals show multiple zonations (Figure 2b), with sieve-textured zones at  $\text{An}_{87-91}$  (like the anorthite-rich plagioclase hosted in LP melt), and homogeneous zones at  $\text{An}_{76-78}$ . These lower An-contents occur always in the outermost rims of the crystals, where they are in contact with the HP melt. The olivines in the HP magma show no zonations with  $\text{Mg\#} = 69$ . Clinopyroxenes form large grains with diameters up to 5 mm. Large grains contain melt and mineral inclusions, which are indistinguishable from the phases  
20 observed in the HP magma (Figure 2c). Some pyroxenes contain antecryst cores ( $\text{Mg\#} = 71$ ), occasionally with diopsidic rims ( $\text{Mg\#} = 89$ ). For a detailed discussion of these textural and compositional features in the clinopyroxenes see Di Stefano et al. (2020).

The texture of mingled LP and HP magma is shown in the mineral map of sample S3 in Figure 3. The sample contains 25% glass (15% LP and 10% HP), 64% bubbles, 8% plagioclase, 1% olivine, and 2% clinopyroxene. The MLA map  
25 shows sharp contacts of the two glass phases (Figure 3c). Even at sharp boundaries the method allows a clear distinction between the different glass phases, despite their chemical similarity (Table 1). The sharp contacts evident in the MLA map suggest that no significant diffusional exchange between the LP and HP magmas occurred prior to the paroxysmal eruption.

30

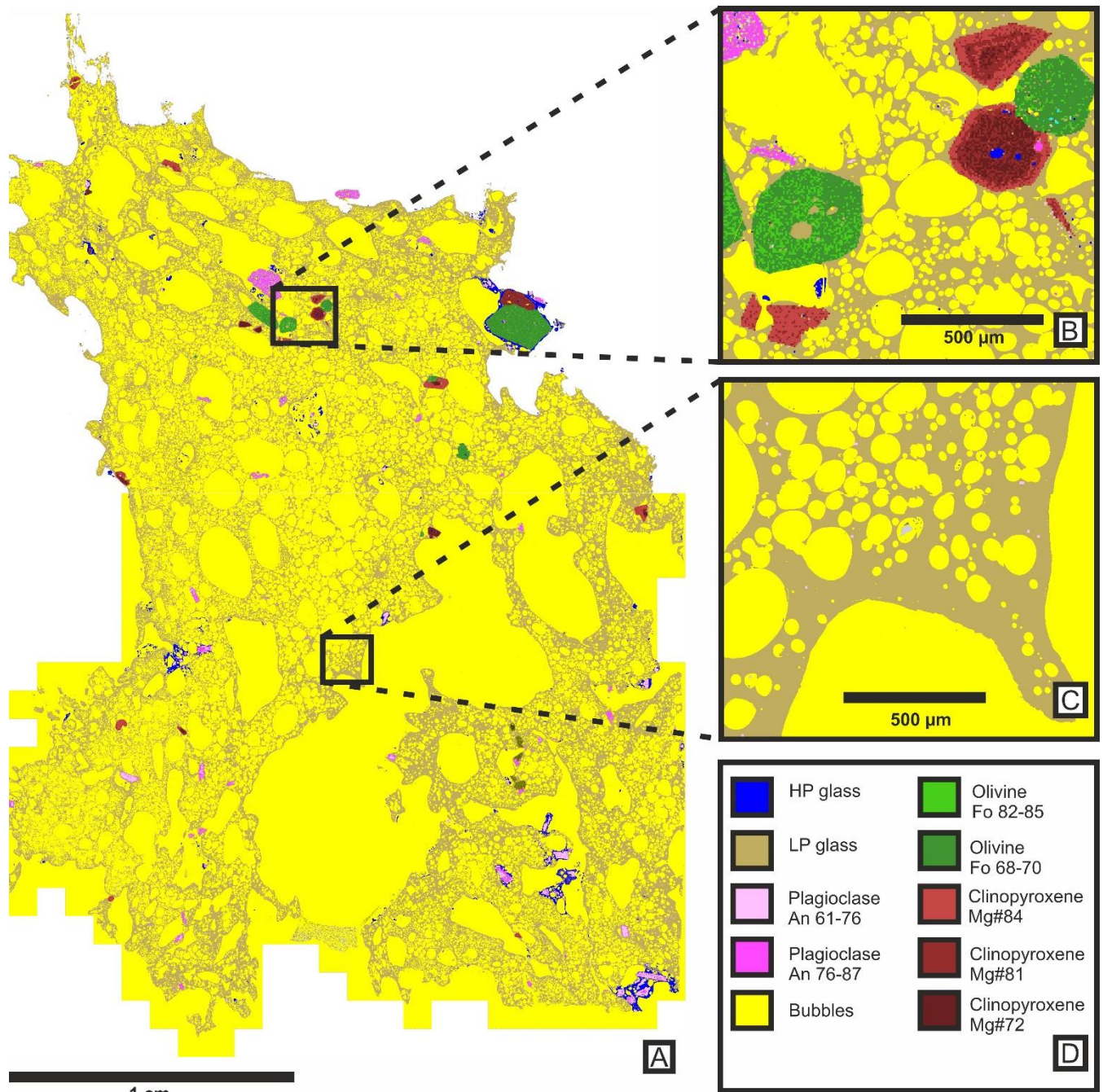


**Figure 1: MLA map of thin section S1, representing the LP endmember magma. This magma is very crystal poor and bubble rich. B) Magnified area shows plagioclase (pink), olivine (green), and clinopyroxene (red) hosted in the LP magma. The clinopyroxenes show distinct zonations; C) Magnification of crystal-free and bubble-rich LP magma.**

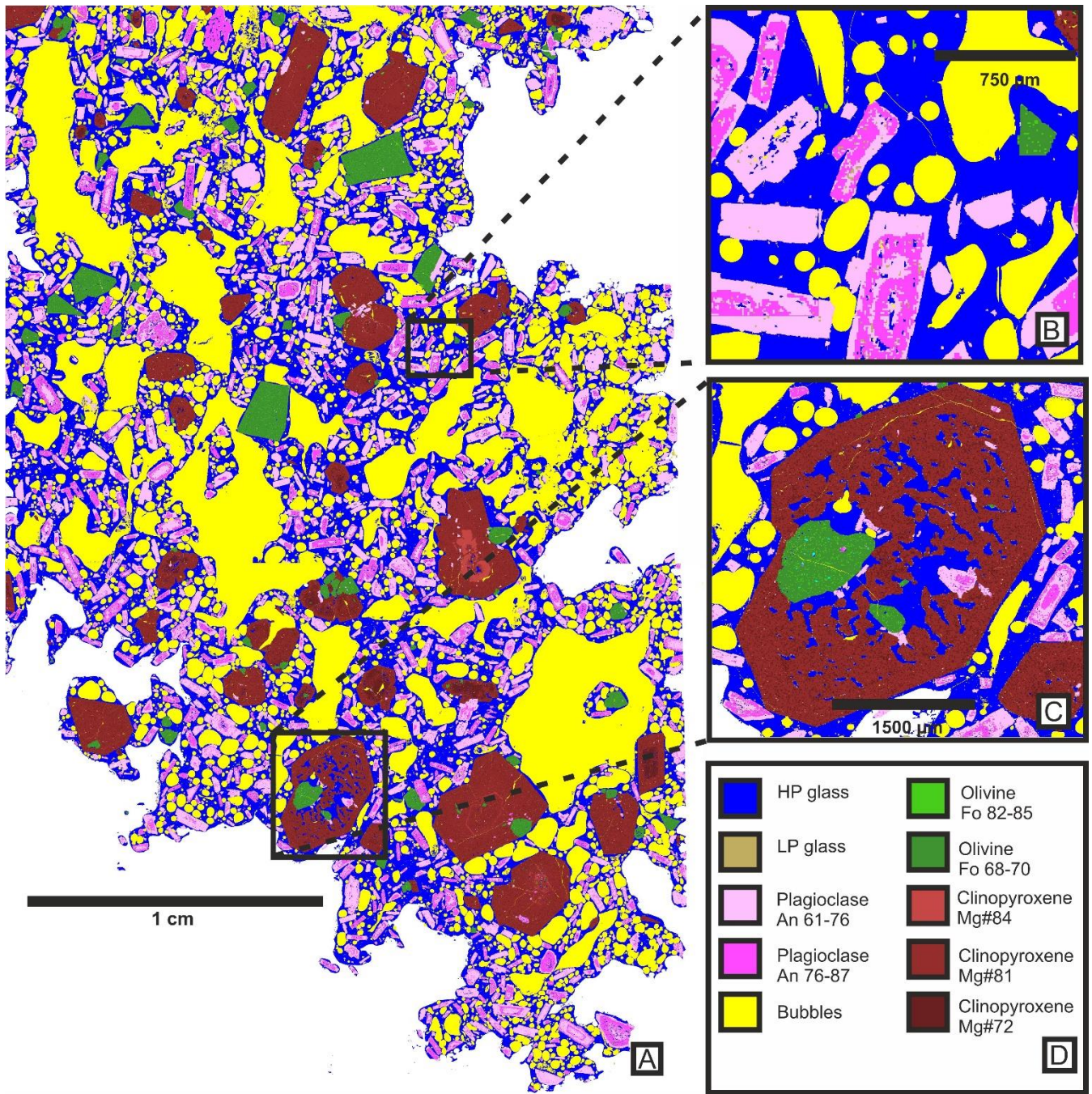


Figure 2 : MLA map of the HP endmember magma, thin section S4. HP glass is shown in blue, bubbles in yellow, plagioclase in pink, olivine in green, and clinopyroxene in dark-red. B) Magnified area shows zonations in plagioclase crystals; C) Large clinopyroxene grain (Mg# ~ 74) with HP melt inclusions, and plagioclase and olivine mineral inclusions.

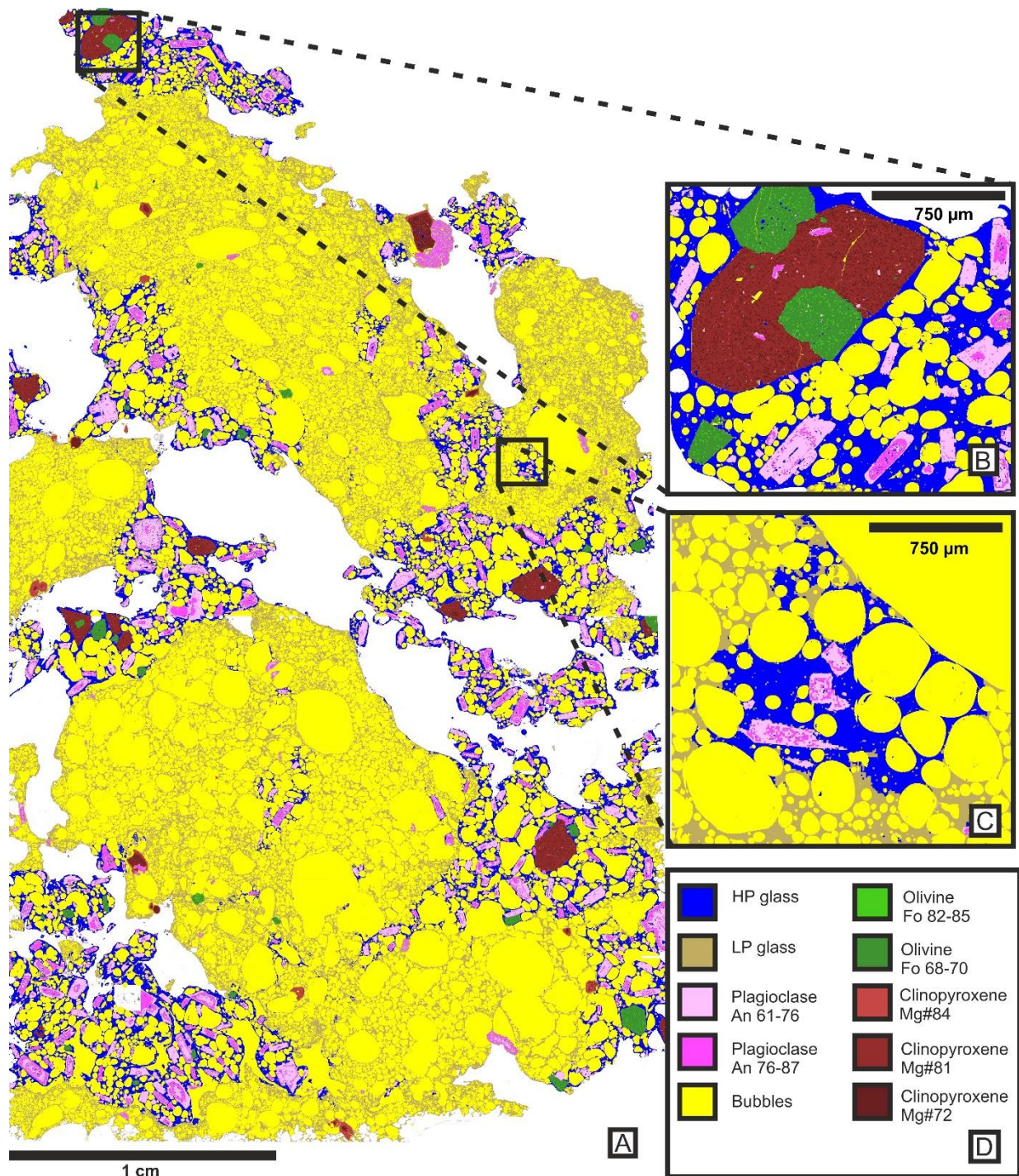


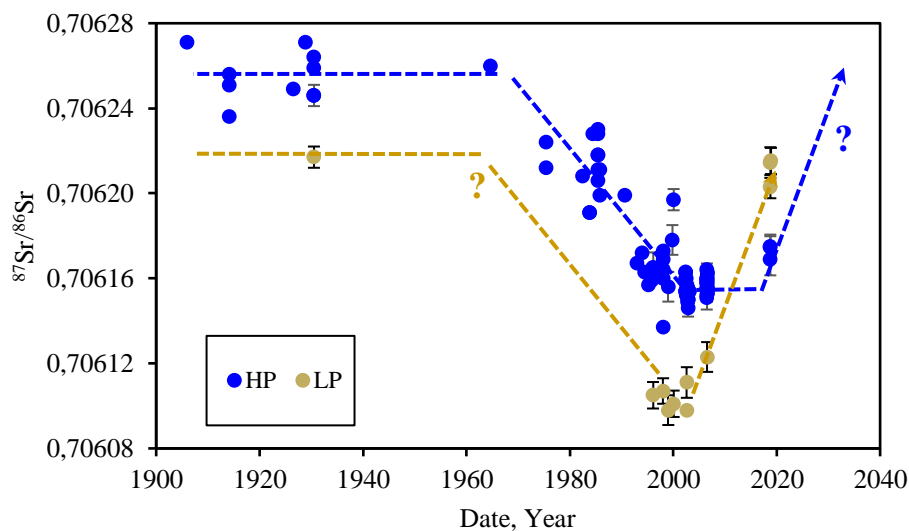
Figure 3: MLA map of thin section S3 representing a sample with mingled LP and HP magma. A) overview image of the entire thin section; B) Area with HP magma; C) Contact between LP and HP magma shows no diffusive exchange.

**Table 1: Major and trace element compositions of the end-member HP (n=17) and LP (n=12) glasses measured in thin sections of eruption products from the paroxysm in July 2019. Oxides and Cl are reported in wt.%, and the trace elements are reported in µg/g.**

	HP glass	s.e.	Lp glass	s.e.
SiO <sub>2</sub>	52.16	0.59	48.57	0.59
TiO <sub>2</sub>	1.63	0.02	0.93	0.01
Al <sub>2</sub> O <sub>3</sub>	15.23	0.08	17.65	0.08
FeO <sub>(tot)</sub>	10.06	0.22	8.16	0.15
MnO	0.195	0.010	0.159	0.008
MgO	3.43	0.09	5.97	0.08
CaO	7.06	0.17	11.02	0.37
Na <sub>2</sub> O	3.32	0.17	2.40	0.34
K <sub>2</sub> O	4.12	0.10	2.00	0.15
Cl	0.120	0.004	0.117	0.004
V <sub>2</sub> O <sub>3</sub>	0.120	0.005	0.083	0.007
Total	97.74	0.62	97.28	0.74
Mg#	37.80	0.56	56.58	0.40
Cl	1198	38	1172	41
S	368	27	416	46
Sc	23.7	0.8	27.8	0.7
Co	26.7	0.9	31.5	1.1
Ni	10.6	0.8	36.1	2.5
Cu	209	48	100	31
Zn	118.4	2.6	82.6	5.6
As	9.63	0.53	b.d.l.	
Rb	136.5	6.6	54.8	1.5
Sr	519	28	661	15
Y	39.1	1.4	19.9	1.2
Zr	282.1	9.9	116.8	6.3
Nb	38.2	1.3	15.0	0.4
Mo	3.1	0.4	1.3	0.2
Sn	2.8	0.3	1.3	0.2
Cs	9.3	0.5	3.6	0.1
Ba	1576	44	857	25
La	78.4	13.7	36.5	0.9
Ce	157.3	27.1	75.8	2.2
Pr	17.8	3.2	8.8	0.3
Nd	71.1	2.5	35.6	1.2
Sm	13.3	0.5	6.7	0.4
Eu	3.04	0.14	1.86	0.09
Gd	10.3	0.5	5.4	0.3
Tb	1.40	0.07	0.75	0.05
Dy	7.9	0.4	4.2	0.3
Ho	1.49	0.08	0.76	0.07
Er	4.1	0.1	2.1	0.1
Tm	0.56	0.03	0.28	0.06
Yb	3.8	0.3	2.0	0.1
Lu	0.56	0.02	0.28	0.02
Hf	6.5	0.3	2.8	0.2
Ta	1.97	0.09	0.76	0.06
W	4.04	0.25	1.51	0.12
Tl	0.17	0.02	0.21	0.05
Pb	30.6	1.4	16.8	4.3
Bi	0.05	0.01	0.13	0.13
Th	29.3	1.1	10.8	0.5
U	8.10	0.28	2.94	0.09

**Table 2:  $^{87}\text{Sr}/^{86}\text{Sr}$ ,  $^{143}\text{Nd}/^{144}\text{Nd}$ ,  $^{206}\text{Pb}/^{204}\text{Pb}$ ,  $^{207}\text{Pb}/^{204}\text{Pb}$ ,  $^{208}\text{Pb}/^{204}\text{Pb}$ , and  $^{176}\text{Hf}/^{177}\text{Hf}$  isotopic ratios of LP and HP material erupted in the paroxysmal eruptions in 2019.**

eruption date	sample name	material	magma phase	$^{87}\text{Sr}/^{86}\text{Sr}$	2 s.e.	$^{143}\text{Nd}/^{144}\text{Nd}$	2 s.e.	$^{206}\text{Pb}/^{204}\text{Pb}$	2 s.e.
15.08.2019	LP_S.V._2019-08-15	Pumice	LP	0.706215	0.000006	0.512584	0.000008	19.079	0.001
03.07.2019	LP2_2019-07-03	Pumice	LP	0.706203	0.000005	0.512584	0.000008	19.077	0.001
03.07.2019	LP_2019-07-03	Pumice	LP	0.706214	0.000007	0.512569	0.000008	19.083	0.001
03.07.2019	HP2_2019-07-03	scoria	HP	0.706175	0.000005	0.512564	0.000007	19.086	0.001
03.07.2019	HP_flow_2019-07-03	lava flow	HP	0.706175	0.000006	0.512580	0.000007	19.085	0.001
03.07.2019	HP_2019-07-03	scoria	HP	0.706169	0.000007	0.512574	0.000007	19.077	0.001
				$^{207}\text{Pb}/^{204}\text{Pb}$	2 s.e.	$^{208}\text{Pb}/^{204}\text{Pb}$	2 s.e.	$^{176}\text{Hf}/^{177}\text{Hf}$	2 s.e.
15.08.2019	LP_S.V._2019-08-15	Pumice	LP	15.685	0.001	39.129	0.003	0.282863	0.000005
03.07.2019	LP2_2019-07-03	Pumice	LP	15.682	0.001	39.118	0.003	0.282865	0.000006
03.07.2019	LP_2019-07-03	Pumice	LP	15.689	0.001	39.142	0.002	0.282851	0.000008
03.07.2019	HP2_2019-07-03	scoria	HP	15.690	0.001	39.148	0.003	0.282846	0.000010
03.07.2019	HP_flow_2019-07-03	lava flow	HP	15.690	0.001	39.145	0.002	0.282852	0.000006
03.07.2019	HP_2019-07-03	scoria	HP	15.687	0.001	39.131	0.004	0.282848	0.000005



- 5 **Figure 4: Evolution of the  $^{87}\text{Sr}/^{86}\text{Sr}$  isotopic ratio of the HP and LP magmas over the past 120 years. Uncertainties are plotted where available from the literature. The HP magma erupted in 2019 has not changed significantly since the previous paroxysms in 2007. However, the LP magma erupted in 2019 shows a major shift to a more radiogenic composition, similar to that of the LP magma erupted in 1930. The isotopic data for erupted materials previous to 2019 are compiled from the literature (Bertagnini et al. 2008; Francalanci et al. 1999, 2005, 2004).**

In addition to the samples documented by MLA, major and trace element analysis, we measured the isotopic compositions of a lava flow sample (HP) that formed as a secondary flow in the July paroxysm, and scoria sample from the August 28<sup>th</sup> 2019 paroxysm (LP). Table 2 lists the measured isotopic compositions of these samples. The isotopic systems reported here are  $^{87}\text{Sr}/^{86}\text{Sr}$ ,  $^{143}\text{Nd}/^{144}\text{Nd}$ ,  $^{206}\text{Pb}/^{204}\text{Pb}$ ,  $^{207}\text{Pb}/^{204}\text{Pb}$ ,  $^{208}\text{Pb}/^{204}\text{Pb}$ , and  $^{176}\text{Hf}/^{177}\text{Hf}$ .

5 Francalanci et al. 2008 reported a Nd isotope ratio for both LP pumice and HP scoria erupted on April 5<sup>th</sup> 2003 of 0.51257, which is indistinguishable from the materials erupted in 2019, as well as eruption products from 1996 and 1999 (Francalanci et al. 2004). The  $^{143}\text{Nd}/^{144}\text{Nd}$  isotope ratio shows no resolvable difference between the LP and HP magmas. Similarly, Pb- and Hf-isotope ratios show no systematic differences between the two magmas (Table 2).

10 The Sr-isotopic system shows a clear difference between the bulk compositions of the LP and HP magmas. In the samples erupted in 2019 the LP magma has a higher  $^{87}\text{Sr}/^{86}\text{Sr}$  ratio by approximately  $4.6 \times 10^{-5}$  compared to the HP bulk isotopic composition (Figure 4). This offset is an order of magnitude larger than the analytical error. This is in contrast to Sr-isotopic ratios measured in older eruption products, in which the HP magma had a systematically higher ratio compared to the LP magma (Bertagnini et al. 2008; Francalanci et al. 1999, 2005, 2004). A time resolved representation of the  
15  $^{87}\text{Sr}/^{86}\text{Sr}$  values reveals, that the isotopic composition of the HP magma has remained unchanged from the previous paroxysms until 2007, whereas the ratio of the LP magma has increased to a higher value last recorded in 1930 (Figure 4). This jump in the isotopic composition suggests a shift in the deep magmatic feeding system leading to the paroxysms in 2019, which we discuss below.

## 20 4 DISCUSSION

The systematically higher  $^{87}\text{Sr}/^{86}\text{Sr}$  of the HP magma compared to the LP magma prior to 2019 has been explained by the presence of an old cumulus reservoir with abundant plagioclase and clinopyroxene and a high  $^{87}\text{Sr}/^{86}\text{Sr}$ . This crystal mush is occurring at intermediate depths between the deep LP magma reservoir (~11 km) and the shallow HP magma reservoir (~3 km). As fresh crystal-poor and volatile-rich LP magma rises to the upper HP reservoir it assimilates high  
25  $^{87}\text{Sr}/^{86}\text{Sr}$  cumulus material, leading to a higher  $^{87}\text{Sr}/^{86}\text{Sr}$  in the HP magma and isotopic disequilibrium in zoned plagioclase and clinopyroxene grains (Francalanci et al. 2005, 2008).

The shift to lower  $^{87}\text{Sr}/^{86}\text{Sr}$  recorded after 1970 are however not explained by evolving interactions of the LP magma with an intermediate cumulus mush. Since the LP magma feeds the HP reservoir, it is likely that the change in Sr isotope ratios originates in the deep LP source at a depth of 11 km or so. A change in  $^{87}\text{Sr}/^{86}\text{Sr}$  could be explained by variations  
30 in the degree of crustal contamination with time, whereas a higher  $^{87}\text{Sr}/^{86}\text{Sr}$  would suggest more contamination. However, such a significant and evolving degree of crustal contamination should be noticeable in the trace element signatures, which is not the case over the past 100 years (Francalanci et al. 2008). Instead, Francalanci et al. (1999)

suggested that the shift to lower  $^{87}\text{Sr}/^{86}\text{Sr}$  originated prior to 1980 with a pulse of fresh magma input in the LP reservoir, followed by the slow isotopic re-equilibration of the HP reservoir over a period of 20 years until the mid-1990s.

Here, we propose that this pulse of fresh magma with a low  $^{87}\text{Sr}/^{86}\text{Sr}$  into the LP reservoir has been consumed, either by eruption or storage in the system, leading to a LP magma  $^{87}\text{Sr}/^{86}\text{Sr}$  equivalent to that prior to the fresh input. The 2019  
5 paroxysms sample a moment in the magmatic evolution of Stromboli, where the deep LP reservoir has returned to a state equivalent to that prior of 1980, sampled by the major paroxysm of 1930, but the upper HP reservoir has not had the time to isotopically re-equilibrate. A shift in the magmatic source behavior of the paroxysms in 2019 compared to 2003-  
2017 was also observed in the clinopyroxene population (Petroni et al. 2022). Petroni et al. (2022) suggested that the 2019 paroxysms were fed by a rejuvenated plumbing system with a lower degree of crystal mush assimilation compared  
10 to earlier eruptions. This lack of mush remobilization is seen in the absence of changes in the HP magma  $^{87}\text{Sr}/^{86}\text{Sr}$ , despite the increase observed for the LP magma.

In conclusion, we propose that, assuming the rate of mass transport remains unchanged, the HP reservoir can be expected to evolve to an  $^{87}\text{Sr}/^{86}\text{Sr}$  of  $\sim 0.70626 \pm 0.00002$  over the next  $\sim 20$  years. A continuous and systematic sampling and measurement of Sr isotope ratios will thus provide a key to the assessment of magma input rates into the HP reservoir  
15 and the volume of it.

#### AUTHOR CONTRIBUTIONS

Renggli: Conceptualization, investigation, resources, formal analysis, writing – original draft. Krause: Conceptualization, investigation, resources, formal analysis, writing – review & editing. Genske: investigation, writing  
20 – review & editing. Gilbricht: investigation. Gattuso: resources. Böhnke: investigation. Berndt: investigation. Giuffrida: resources.

#### ACKNOWLEDGEMENTS

CR is funded by the Deutsche Forschungsgemeinschaft (DFG, German Research Foundation) – project 442083018. We  
25 thank B. Schmitte and M. Trogisch for help and support in the laboratories at the Institut für Mineralogie, University of Münster.

#### DATA AVAILABILITY

The data is publicly available on the DIGIS Geochemical Data Repository: Renggli, Christian; Krause, Joachim; Genske, Felix; Gilbricht, Sabine; Gattuso, Alessandro; Böhnke, Mischa; Berndt, Jasper; Giuffrida, Giovanni (2023): Radiogenic  
30 isotope compositions of eruption products from the 2019 paroxysmal eruptions at Stromboli Volcano. GFZ Data Services. <https://doi.org/10.5880/digis.2023.007>

## REFERENCES

References should be included at the end of the manuscript, in APA style: <http://www.bibme.org/citation-guide/apa/>

### Where possible, DOI numbers should be provided.

- 5 Allard, P. 2010. “A CO<sub>2</sub>-Rich Gas Trigger of Explosive Paroxysms at Stromboli Basaltic Volcano, Italy.” *Journal of Volcanology and Geothermal Research* 189(3):363–74. doi: 10.1016/j.jvolgeores.2009.11.018.
- Armienti, P., L. Francalanci, and P. Landi. 2007. “Textural Effects of Steady State Behaviour of the Stromboli Feeding System.” *Journal of Volcanology and Geothermal Research* 160(1):86–98. doi: 10.1016/j.jvolgeores.2006.05.004.
- 10 Bertagnini, A., N. Métrich, P. Landi, and M. Rosi. 2003. “Stromboli Volcano (Aeolian Archipelago, Italy): An Open Window on the Deep-Feeding System of a Steady State Basaltic Volcano.” *Journal of Geophysical Research: Solid Earth* 108(B7). doi: 10.1029/2002JB002146.
- Bertagnini, A., M. Coltelli, P. Landi, M. Pompilio, and M. Rosi. 1999. “Violent Explosions Yield New Insights into Dynamics of Stromboli Volcano.” *EOS Transactions* 80:633–36. doi: 10.1029/99EO00415.
- 15 Bertagnini, A., N. Métrich, L. Francalanci, P. Landi, S. Tommasini, and S. Conticelli. 2008. “Volcanology and Magma Geochemistry of the Present-Day Activity: Constraints on the Feeding System.” *Geophysical Monograph Series*, 182:19–37. doi: 10.1029/182GM04.
- Bevilacqua, A., A. Bertagnini, M. Pompilio, P. Landi, P. Del Carlo, A. Roberto, W. Aspinall, and A. Neri. 2020. “Major Explosions and Paroxysms at Stromboli (Italy): A New Historical Catalog and Temporal Models of Occurrence with Uncertainty Quantification.” *Scientific Reports* 10. doi: 10.1038/s41598-020-74301-8.
- 20 Blichert-Toft, J., C. Chauvel, and F. Albarède. 1997. “Separation of Hf and Lu for High-Precision Isotope Analysis of Rock Samples by Magnetic Sector-Multiple Collector ICP-MS.” *Contributions to Mineralogy and Petrology* 127(3):248–60. doi: 10.1007/s004100050278.
- Di Stefano, F., S. Mollo, T. Ubide, C. M. Petrone, J. Caulfield, P. Scarlato, M. Nazzari, D. Andronico, and E. Del Bello. 2020. “Mush Cannibalism and Disruption Recorded by Clinopyroxene Phenocrysts at Stromboli Volcano: New Insights from Recent 2003–2017 Activity.” *Lithos* 360–361:105440. doi: 10.1016/j.lithos.2020.105440.
- D’Oriano, C., A. Bertagnini, and M. Pompilio. 2011. “Ash Erupted during Normal Activity at Stromboli (Aeolian Islands, Italy) Raises Questions on How the Feeding System Works.” *Bulletin of Volcanology* 73(5):471–77. doi: 10.1007/s00445-010-0425-0.
- 30 Francalanci, L., A. Bertagnini, N. Metrich, A. Renzulli, R. Vannucci, P. Landi, S. Del Moro, M. Menna, C. M. Petrone, and I. Nardini. 2008. “Mineralogical, Geochemical, and Isotopic Characteristics of the Ejecta from the 5 April 2003 Paroxysm at Stromboli, Italy: Inferences on the Pre-ruptive Magma Dynamics.” *Geophysical Monograph Series*, 182:331–345. doi:10.1029/182GM27.
- 35 Francalanci, L., G. R. Davies, W. Lustenhouwer, S. Tommasini, P. R. D. Mason, and S. Conticelli. 2005. “Intra-Grain Sr Isotope Evidence for Crystal Recycling and Multiple Magma Reservoirs in the Recent Activity of Stromboli Volcano, Southern Italy.” *Journal of Petrology* 46(10):1997–2021. doi: 10.1093/petrology/egi045.

- 5 Francalanci, L., S. Tommasini, and S. Conticelli. 2004. "The Volcanic Activity of Stromboli in the 1906–1998 AD Period: Mineralogical, Geochemical and Isotope Data Relevant to the Understanding of the Plumbing System." *Journal of Volcanology and Geothermal Research* 131(1):179–211. doi: 10.1016/S0377-0273(03)00362-7.
- 5 Francalanci, L., S. Tommasini, S. Conticelli, and G. R. Davies. 1999. "Sr Isotope Evidence for Short Magma Residence Time for the 20th Century Activity at Stromboli Volcano, Italy." *Earth and Planetary Science Letters* 167(1):61–69. doi: 10.1016/S0012-821X(99)00013-8.
- Genske, F. S., S. P. Turner, C. Beier, and B. F. Schaefer. 2012. "The Petrology and Geochemistry of Lavas from the Western Azores Islands of Flores and Corvo." *Journal of Petrology* 53(8):1673–1708. doi: 10.1093/petrology/egs029.
- 10 Jochum, K. P., U. Nohl, K. Herwig, E. Lammel, B. Stoll, and A. W. Hofmann. 2005. "GeoReM: A New Geochemical Database for Reference Materials and Isotopic Standards." *Geostandards and Geoanalytical Research* 29(3):333–38. doi: 10.1111/j.1751-908X.2005.tb00904.x.
- 15 Landi, P., L. Francalanci, R. A. Corsaro, C. M. Petrone, A. Fornaciai, M. R. Carroll, I. Nardini, and L. Miraglia. 2008. "Textural and Compositional Characteristics of Lavas Emitted During the December 2002 to July 2003 Stromboli Eruption (Italy): Inferences on Magma Dynamics." *Geophysical Monograph Series*, 182:213–228. doi:10.1029/182GM18
- 20 Landi, P., L. Francalanci, M. Pompilio, M. Rosi, R. A. Corsaro, C. M. Petrone, I. Nardini, and L. Miraglia. 2006. "The December 2002–July 2003 Effusive Event at Stromboli Volcano, Italy: Insights into the Shallow Plumbing System by Petrochemical Studies." *Journal of Volcanology and Geothermal Research* 155(3):263–84. doi: 10.1016/j.jvolgeores.2006.03.032.
- Landi, P., N. Métrich, A. Bertagnini, and M. Rosi. 2004. "Dynamics of Magma Mixing and Degassing Recorded in Plagioclase at Stromboli (Aeolian Archipelago, Italy)." *Contributions to Mineralogy and Petrology* 147(2):213–27. doi: 10.1007/s00410-004-0555-5.
- 25 Lautze, N. C., and B. F. Houghton. 2005. "Physical Mingling of Magma and Complex Eruption Dynamics in the Shallow Conduit at Stromboli Volcano, Italy." *Geology* 33(5):425–28. doi: 10.1130/G21325.1.
- Lugmair, G. W., and S. J. G. Galer. 1992. "Age and Isotopic Relationships among the Angrites Lewis Cliff 86010 and Angra Dos Reis." *Geochimica et Cosmochimica Acta* 56(4):1673–94. doi: 10.1016/0016-7037(92)90234-A.
- 30 Métrich, N., A. Bertagnini, P. Landi, and M. Rosi. 2001. "Crystallization Driven by Decompression and Water Loss at Stromboli Volcano (Aeolian Islands, Italy)." *Journal of Petrology* 42(8):1471–90. doi: 10.1093/petrology/42.8.1471.
- Métrich, N., A. Bertagnini, P. Landi, M. Rosi, and O. Belhadj. 2005. "Triggering Mechanism at the Origin of Paroxysms at Stromboli (Aeolian Archipelago, Italy): The 5 April 2003 Eruption." *Geophysical Research Letters* 32(10). doi: 10.1029/2004GL022257.
- 35 Métrich, N., A. Bertagnini, and A. Di Muro. 2010. "Conditions of Magma Storage, Degassing and Ascent at Stromboli: New Insights into the Volcano Plumbing System with Inferences on the Eruptive Dynamics." *Journal of Petrology* 51(3):603–26. doi: 10.1093/petrology/egp083.

- Münker, C., S. Weyer, E. Scherer, and K. Mezger. 2001. "Separation of High Field Strength Elements (Nb, Ta, Zr, Hf) and Lu from Rock Samples for MC-ICPMS Measurements." *Geochemistry, Geophysics, Geosystems* 2(12). doi: 10.1029/2001GC000183.
- 5 Osbahr, I., J. Krause, K. Bachmann, and J. Gutzmer. 2015. "Efficient and Accurate Identification of Platinum-Group Minerals by a Combination of Mineral Liberation and Electron Probe Microanalysis with a New Approach to the Offline Overlap Correction of Platinum-Group Element Concentrations\*." *Microscopy and Microanalysis* 21(5):1080–95. doi: 10.1017/S1431927615000719.
- 10 Petrone, C. M., S. Mollo, R. Gertisser, Y. Buret, P. Scarlato, E. Del Bello, D. Andronico, B. Ellis, A. Pontesilli, G. De Astis, P. P. Giacomoni, M. Coltorti, and M. Reagan. 2022. "Magma Recharge and Mush Rejuvenation Drive Paroxysmal Activity at Stromboli Volcano." *Nature Communications* 13(1):7717. doi: 10.1038/s41467-022-35405-z.
- Pin, C., and Zalduegui, J. F. S. 1997. "Sequential Separation of Light Rare-Earth Elements, Thorium and Uranium by Miniaturized Extraction Chromatography: Application to Isotopic Analyses of Silicate Rocks." *Analytica Chimica Acta* 339(1):79–89. doi: 10.1016/S0003-2670(96)00499-0.
- 15 Renggli, C. J., J. Krause., F. Genske, S. Gilbricht, A. Gattuso, M. Böhnke, J. Berndt, G. Giuffrida. 2023. Radiogenic isotope compositions of eruption products from the 2019 paroxysmal eruptions at Stromboli Volcano [Dataset]. GFZ Data Services. <https://doi.org/10.5880/digis.2023.007>
- 20 Rosi, M., M. Pistolesi, A. Bertagnini, P. Landi, M. Pompilio, and A. Di Roberto. 2013. "Chapter 14 Stromboli Volcano, Aeolian Islands (Italy): Present Eruptive Activity and Hazards." *Geological Society, London, Memoirs* 37(1):473–90. doi: 10.1144/M37.14.
- Todd, E., A. Stracke, and E. E. Scherer. 2015. "Effects of Simple Acid Leaching of Crushed and Powdered Geological Materials on High-Precision Pb Isotope Analyses." *Geochemistry, Geophysics, Geosystems* 16(7):2276–2302. doi: 10.1002/2015GC005804.
- 25 Viccaro, M., A. Cannata, F. Cannavò, R. De Rosa, M. Giuffrida, E. Nicotra, M. Petrelli, and G. Sacco. 2021. "Shallow Conduit Dynamics Fuel the Unexpected Paroxysms of Stromboli Volcano during the Summer 2019." *Scientific Reports* 11(1):266. doi: 10.1038/s41598-020-79558-7.
- 30 Weis, D., B. Kieffer, C. Maerschalk, J. Barling, J. de Jong, G. A. Williams, D. Hanano, W. Pretorius, N. Mattielli, J. S. Scoates, A. Goolaerts, R. M. Friedman, and J. B. Mahoney. 2006. "High-Precision Isotopic Characterization of USGS Reference Materials by TIMS and MC-ICP-MS." *Geochemistry, Geophysics, Geosystems* 7(8). doi: 10.1029/2006GC001283.